RSC Advances

ROYAL SOCIETY OF CHEMISTRY

www.rsc.org/advances

Journal Name

RSCPublishing

ARTICLE

Mesoporous SnO_2 nanoparticle films as electron-transporting material in perovskite solar cells

Cite this: DOI: 10.1039/xoxxoooooox

Yi Li,[1,2] Jun Zhu,[1]* Yang Huang,[1]Feng liu,[1] Mei lv,[1] Shuanghong Chen,[1] Linhua Hu,[1] Junwang Tang,[3]* Jianxi Yao,[4] and Songyuan Dai[1,4,]*

Received ooth January 2012,
Accepted ooth January 2012

DOI: 10.1039/xoxxoooooox

www.rsc.org/

Perovskite solar cells with mesoporous metal oxide films as scaffold layers have been demonstrated very impressive advances in performance recently. Here, we present an investigation into mesoporous perovskite solar cells incorporating mesoporous SnO_2 nanoparticle films as electron-transporting materials and scaffold layers, to replace the traditional mesoporous TiO_2 films. By optimizing the SnO_2 film thickness and treating the surface of SnO_2 film with $TiCl_4$ aqueous solution. Due to the $TiCl_4$ treatment significantly retards the recombination process, the short-circuit current density (J_{sc}) and open-circuit voltage (V_{oc}) reached to nearly 18 mA cm^{-2} and 1 V, respectively. Consequently, the power conversion efficiency of device with SnO_2 film exceeding 10%.

1. Introduction

Organic-inorganic halide lead perovskite ($CH_3NH_3PbX_3$, X = Cl, Br, I) materials have shown great potential in thin-film photovoltaic devices owing to their excellent light absorption coefficient, the appropriate band gap, long diffusion length, and the ease to fabricate these materials with solution process.[1-11] Recently, the power conversion efficiencies (PCEs) of the mesoporous perovskite solar cells have skyrocketed from 3.8% to more than 20% in within 5 years.[1, 5, 10, 11] In the perovskite solar cells based on the mesoporous configuration, mesoporous metal oxide thin films are used as either electron-transporting materials (ETMs) to accept photogenerated electrons from perovskites and then transmitted them to the conductive substrates or mesoporous scaffold layers for perovskite materials formation. Mesoporous TiO_2 nanoparticle film is usually used as ETMs and scaffold layer for high-efficiency perovskite solar cells. Excepting for mesoporous TiO_2 films, a variety of materials are applied into the perovskite solar cells as ETMs and/or the scaffold. For example, one-dimensional TiO_2 nanowires, rutile TiO_2 nanorods, ZnO nanorods, [6,6]-phenyl-C61-butyric acid methyl ester (PCBM), Al_2O_3 and ZrO_2, etc. are successfully introduced into the mesoporous solar cells with different PCEs.[12-18] Despite the remarkable achievement in perovskite solar cells, development of alternative ETMs/scaffold to TiO_2 is a promising avenue to further improve the performance of perovskite solar cells.

Previously, mesoporous tin oxide (SnO_2) thin film electrodes were widely applied in dye-sensitized solar cells (DSCs) as ETMs.[19, 20] SnO_2 has a deeper conduction band than TiO_2 and in principle should facilitate more efficient photo-generated electrons transfer from perovskite light absorber to SnO_2 conduction band.[21] Furthermore, bulk SnO_2 has an electron mobility of up to 240 $cm^2 V^{-1} s^{-1}$, which is 100 times higher than that of TiO_2,[22] making it conceptually a more likely candidate for highly efficient solar cells. The DSCs based on SnO_2 electrodes usually give lower PCE compared to those of TiO_2 electrodes, due to the serious recombination between the "bare" SnO_2 with the hole-transporting materials (HTMs).[19] However, by treating the surface of the SnO_2 nanoparticles with $TiCl_4$ aqueous solution or wide band gap "insulating"oxides, such as MgO or Al_2O_3, suppression of the back reaction enable a significant enhancement in PCE of DSCs over 7%.[23] There are still no reports about mesoporous SnO_2 as ETMs in perovskite solar cells despite the distinguished advantages. In this study, we present perovskite solar cells utilizing mesoporous SnO_2 electrodes as the ETMs. By optimizing thickness of the SnO_2 film and treating the surface of the SnO_2 film with $TiCl_4$ aqueous solution, the short-circuit current density and open-circuit voltage have been increased to nearly 18 mA/cm^2 and 1 V, respectively, resulting in devices with over 10% PCE. Furthermore, we employed impedance spectroscopy (IS) to investigate the recombination kinetics of devices based on mesoporous SnO_2 electrodes before and after treating SnO_2 by $TiCl_4$ aqueous solution.

2. Results and discussion

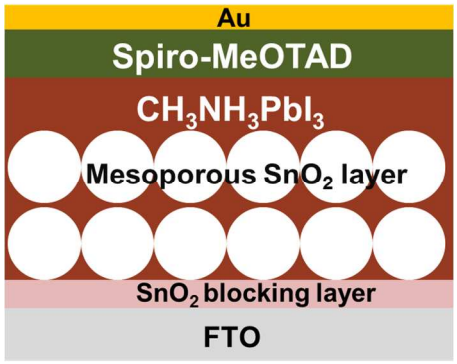

Fig. 1 Schematic device structure of the $CH_3NH_3PbI_3$ perovskite solar cells using mesoporous SnO_2 as ETMs

We present a solid state mesoporous perovskite solar cell incorporating a mesoporous SnO_2 film as ETMs, $CH_3NH_3PbI_3$ as lighting absorber and spiro-MeOTAD as hole-transporting layer. Schematic structure of the device is depicted in Fig. 1. It is imperative for the mesoporous perovskite solar cells to prepare a compact blocking layer to retard the combination of FTO substrate and hole conductor.[24] In this perovskite solar cell, mesoporous SnO_2 thin films are used as both ETMs to accept photogenerated electron from $CH_3NH_3PbI_3$ perovskites and then transmitted to the conductive substrate and mesoporous scaffold layer for perovskite materials formation. We fabricated the $CH_3NH_3PbI_3$ perovskite on the mesoporous SnO_2 films via two-step spin-coating procedure,[25] as shown in Fig. 2. Firstly, the mesoporous SnO_2 film was infiltrated with PbI_2-dissolved DMF solution by spin coating, mesoporous SnO_2 layer is completely covered by PbI_2 overlayer with a thickness about 200 nm, as can be seen in Fig. 2b. Secondly, a 100 μL CH_3NH_3I-dissolved isopropyl alcohol solution was spin-coated on the SnO_2/PbI_2 film. Reaction of PbI_2 with CH_3NH_3I forms void-free $CH_3NH_3PbI_3$ cuboids on the mesoporous SnO_2 film, as shown in Fig. 2c.

In order to investigate the effect of SnO_2 film thickness on the photovoltaic performance of perovskite solar cells, we diluted the spin-coating SnO_2 paste with ethanol in different weight ratio: 1:1; 1:3 and 1:5 to obtain the SnO_2 electrodes with different thickness, and the cross section SEM images of these SnO_2 electrodes were shown in Fig. 3. As can be seen, the thicknesses of these SnO_2 electrodes were 100 nm, 200nm and 300 nm, respectively. Fig. 4 shows the absorption spectra of the $SnO_2/CH_3NH_3PbI_3$ films with SnO_2 thickness of 100 nm, 200nm and 300 nm, respectively. From the results in Fig. 4, the absorption spectra of the $CH_3NH_3PbI_3$ goes up to 800 nm wavelength owing to its bandgap of 1.57 eV. In addition, light absorption is increasing with increasing the thickness of mesoporous SnO_2 films from 100 nm to 300 nm, which is mainly due to further increase of the SnO_2 thickness would increase $CH_3NH_3PbI_3$ deposition amount into the SnO_2 film.

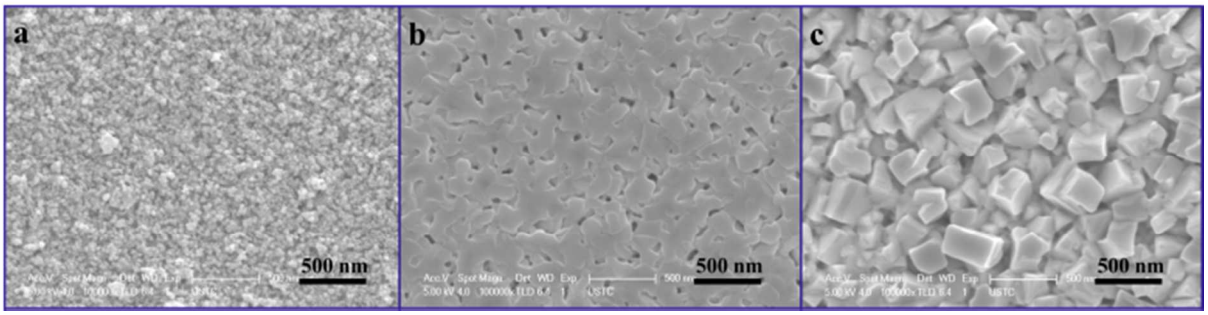

Fig. 2 SEM images of (a) mesoporous SnO_2 film; (b) SnO_2/PbI_2 film; (c) $SnO_2/CH_3NH_3PbI_3$ film. The mesoporous SnO_2 film thickness is about 200 nm.

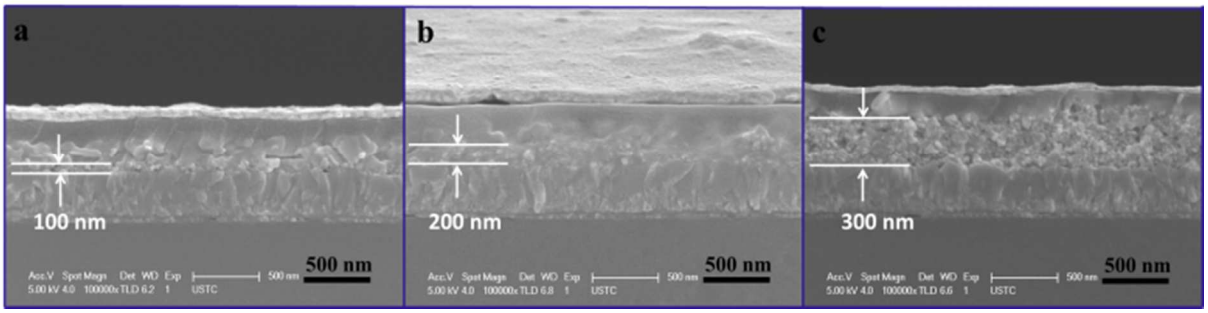

Fig. 3 Cross-sectional SEM images of the mesoporous perovskite solar cells using porous SnO_2 films with different thicknesses as ETMs. SnO_2 films were obtained by spin-coating SnO_2 paste diluted with ethanol to different weight ratio: (a) 1:1; (b) 1:3; (c) 1:5. The structures of the devices are FTO/SnO_2/$CH_3NH_3PbI_3$/spiro-MeOTAD/Au.

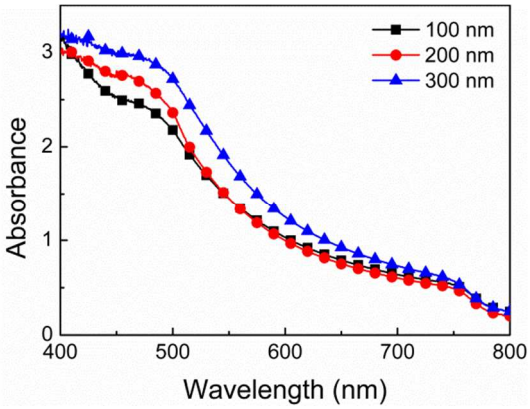

Fig. 4 Effect of different mesoporous SnO_2 films thicknesses on the absorption spectra of $SnO_2/CH_3NH_3PbI_3$ films

Photovoltaic performance of the perovskite solar cells using mesoporous SnO_2 electrode as ETMs were evaluated. Firstly the dependence of photovoltaic performance on the thickness of SnO_2 electrode was investigated. PCE of FTO/SnO_2/$CH_3NH_3PbI_3$/spiro-MeOTAD/Au solar cells is slightly improved from 6.42% (100 nm) to 6.50% (200 nm), which is mainly due to remarkable increase in J_{sc} from 16.78 mA/cm^2 to 18.69 mA/cm^2, though V_{oc} and FF are slightly decreased from 0.753 V and 55.4% (100 nm) to 0.701 V and 53.4% (200 nm), respectively, as shown in Fig. 5a and Table 1. The increased J_{sc} and PCE might arise from the higher light absorption caused by the increased loading of $CH_3NH_3PbI_3$ (Fig. 4). However, with further increasing the thickness of SnO_2 electrode from 200 nm to 300 nm, the PCE of the perovskite solar cells is substantially decreased from 6.50% to 0.90%, which is mainly resulting from significantly decrease in V_{oc}, J_{sc} and FF from 0.701 V, 17.39 mA/cm^2 and 53.4% to 0.272 V, 8.85 mA/cm^2 and 0.373, respectively (as shown in Fig. 5a and Table 1). The decreased efficiency may be explained by a thicker SnO_2 film means a longer distance for charge carriers to go through which also increase the probability of electron-hole recombination. As has been known in the field, the morphology of the perovskite capping layer significantly affects the photovoltaic performance.[25-28] The main reason of effecting PCE for perovskite solar cell is that the thinner $CH_3NH_3PbI_3$ capping layer is prepared on the 300 nm-thick SnO_2 electrode, as can be seen In Fig. 3. In Fig. 5b, the incident photon-to-electron conversion efficiency (IPCE) spectra follows the same trend observed for the short-circuit photocurrent with the SnO_2 based perovskite solar cells. Specially, the perovskite solar cells based on SnO_2 thin film with 200 nm thickness, exhibit an IPCE values of over 80% between 400 to 600 nm. Integrating this IPCE spectra over the AM 1.5 solar spectra at 100mW cm^{-2} estimates a J_{sc} of 17.59 mA/cm^2 in close agreement with our measured maximum value of 17.39 mA/cm^2 under simulated solar conditions.

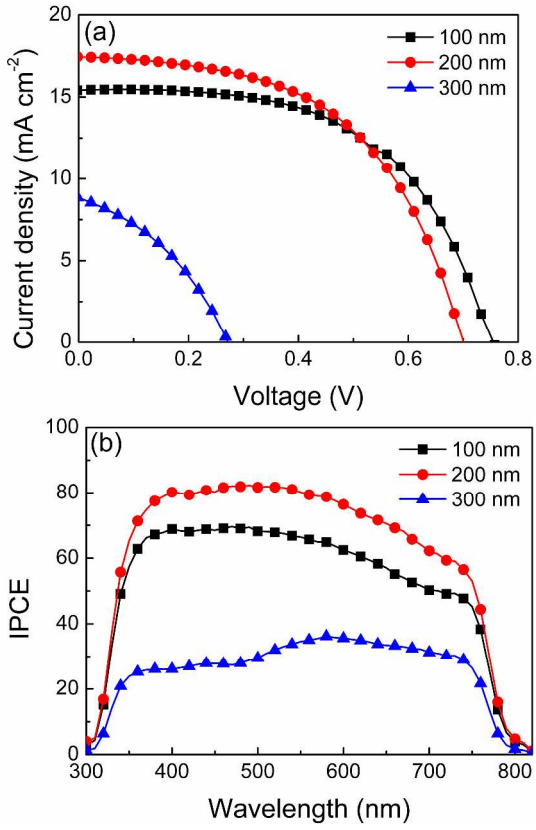

Fig. 5 Effect of the mesoporous SnO_2 thickness on photovoltaic performance of the perovskite solar cells using mesoporous SnO_2 as HTMs (a) and IPCE (b)

Table 1 Photovoltaic performance parameters of the perovskite solar cells depending on the thickness of SnO_2 electrodes.

Thickness of SnO_2 (nm)	V_{oc} (V)[a]	J_{sc} (mA/cm^2)[b]	FF[c]	PCE (%)[d]
100	0.753	15.39	0.554	6.42
200	0.701	17.39	0.534	6.50
300	0.272	8.85	0.373	0.90

[a]Open-circuit photovoltage; [b]Short-circuit photocurrent; [c]Fill factor; [d]Power conversion efficiency.

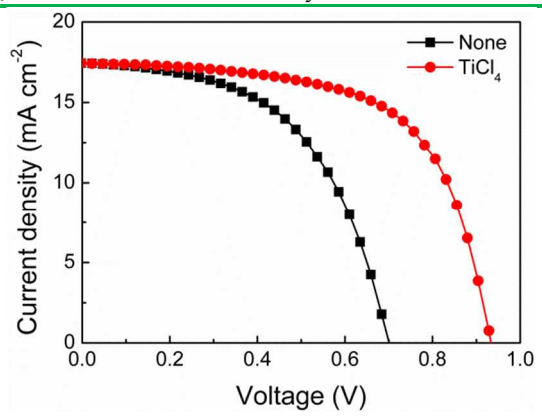

Fig. 6 Current voltage curves for the mesoporous perovskite solar cells with and without treating SnO_2 films surface by $TiCl_4$ aqueous solution. The thickness of SnO_2 electrodes are 200 nm.

Table 2 Photovoltaic performance parameters, Extracted from the current voltage curves presented in Fig. 6.

Surface treatment SnO_2	V_{oc} (V)	J_{sc} (mA/cm^2)	FF	PCE (%)
None	0.701	17.39	0.534	6.50
$TiCl_4$	0.933	17.38	0.628	10.18

For the spiro-MeOTAD-based perovskite solar cell composed of "bare" SnO_2 electrode as ETMs, we found that the performance of this device is unsatisfied, which may cause by the serious electron recombination process between SnO_2 and HTMs or perovskite, In order to inhibit the charge recombination, we optimize the interface between the SnO_2 and perovskite layer via treating by $TiCl_4$ aqueous solution.[24] Photovoltaic performance of the perovskite solar cells with mesoporous SnO_2 electrode with and without treating SnO_2 films surface by $TiCl_4$ aqueous solution were evaluated, as can be seen in Fig. 6 and Table 2. Treating SnO_2 films surface by $TiCl_4$ aqueous solution, PCE of FTO/SnO_2/$CH_3NH_3PbI_3$/spiro-MeOTAD/Au solar cells is substantially improved from 6.50% to 10.18% (33% increment), which is mainly due to significantly increase in V_{oc} from 0.701 V to 0.933 V, with slightly increase in FF from 53.4% to 62.8% and nearly equal J_{sc}.

We employed impedance spectra (IS) to investigate the effect of $TiCl_4$ treatment on the dramatic improvement of the performance of the SnO_2-based perovskite solar cells. Fig. 7a shows representative IS spectra (Nyquist plots) for SnO_2-based perovskite solar cells before and after $TiCl_4$ treatment at low applied forward bias (0.7 V) under dark conditions. The obtained IS includes two arcs, where the first arc in high frequency region is related to the charge transfer behavior at counter electrode and the second arc is due to the combination of the recombination resistance (R_{rec}) and the chemical capacitance of the film (C_μ).[24, 29, 30] Excellent fitting results (Fig. 7a) were obtained using a simplified equivalent circuit (Fig. 7b).[31] R_{rec} for perovskite solar cell incorporating "bare" SnO_2 electrode shows lower value than that incorporating SnO_2 electrode coating an ultrathin TiO_2 layer as the same applied bias voltage, which indicates that recombination process in the device based on TiO_2 coated SnO_2 electrode is remarkably retarded via $TiCl_4$ treatment. Thus, the perovskite solar cells with "bare" SnO_2 electrode represent a lower open-circuit voltage due to higher recombination. Likewise, by treating SnO_2 electrodes surface by $TiCl_4$ aqueous solution, the device shows lower recombination kinetics due to ultrathin TiO_2 between SnO_2 and $CH_3NH_3PbI_3$ layer enabling ease of electron transfer from the TiO_2 to the SnO_2 and also avoid any extra internal trap sites,[24] and thus decrease the charge recombination, leading to 230 mV higher V_{oc} and 10% higher FF than that by the perovskite solar cell incorporating "bare" SnO_2 electrode.

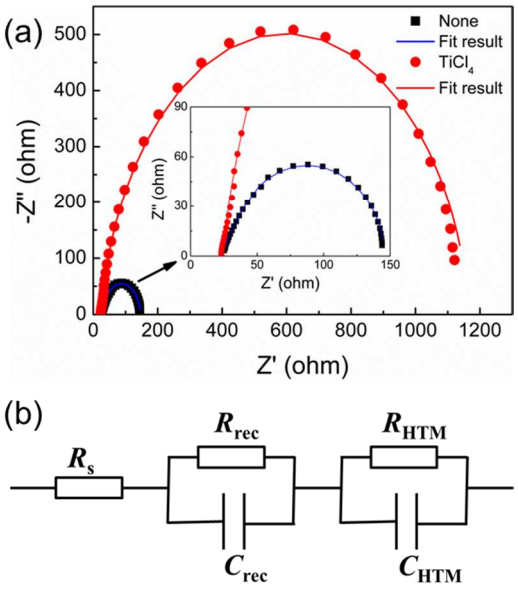

Fig. 7 Nyquist plots for the perovskite solar cells with mesoporous SnO_2 as ETMs before and after treating SnO_2 electrodes surface by $TiCl_4$ aqueous solution, measured under dark condition at 0.7 V biases. The thickness of SnO_2 electrodes is 200 nm. (b) Simplified equivalent circuit model employed for impedance analysis of the perovskite solar cells.

3. Conclusions

In summary, mesoporous SnO_2 film has been successfully utilized in the $CH_3NH_3PbI_3$ perovskite solar cell as electron-transporting material and scaffold layer. By optimizing SnO_2 thickness and treating the surface of the SnO_2 film with $TiCl_4$ aqueous solution, the perovskite solar cell exhibits an increased V_{oc} of around 1 V and a PCE of 10.18%. Impedance spectroscopy results indicated that ultrathin TiO_2 coating the SnO_2 film by $TiCl_4$ treatment significantly retard the charge recombination process via avoid any extra internal trap sites and facilitate electron transfer from the $CH_3NH_3PbI_3$ perovskite to SnO_2 conduction band. These results make the mesoporous SnO_2 based perovskite solar cells competitive with the mesoporous TiO_2 based devices, and a much more promising concept for future optimization of perovskite solar cells.

4. Experimental section

4.1. Materials. Lead (II) iodide (PbI_2, 99%), lithium bis(trifluoromethylsulphonyl) imide (Li-TFSI) (99.95%), 4-tert-butylpyridine (tBP, 96%), butyl-(tin chloride), N,N-dimethylformamide (DMF, 99.9%), hydriodic acid (57 wt% in water) were purchased from Sigma-Aldrich. Methylamine solution (40% in Methanol) was purchased from TCI. Tin (IV) oxide (SnO_2) nanoparticle powders (NanoArc) were purchased from Alfa Aesar and ranged in size from 22 to 43 nm. Spiro-MeOTAD was purchased from Merck KGaA. All chemicals were used as received.

Synthesis of CH_3NH_3I. CH_3NH_3I was synthesized according to the reported method[6]. A hydroiodic acid (30 mL, 57 wt% in water) was reacted with methylamine (27.86 mL, 40% in methanol) in a 250 mL round-bottom flask at 0 °C for 2h. The precipitate was recovered by putting the solution on a rotary

evaporator and carefully removing the solvent at 50 °C for 1 h. The generated yellowish powder was dissolved in ethanol, recrystallized from diethyl ether, and finally dried at 60 °C in a vacuum oven for 24 h.

4.2. Solar cell fabrication.

Substrate preparation: Fluorine-doped tin oxide (FTO, 15Ω /square) glass substrates with dimension of 2 cm × 1.5 cm were partially etched with Zn powder and 2 M HCl to reveal the electrode pattern. The etched substrates were cleaned with detergent, followed by ultrasonicated in pure water and ethanol for 30 min, and then rinsed with deionized water and ethanol, dried by air. Finally, the substrates were annealed at 500 °C for 30 min. A thin (60 nm) blocking layer of SnO_2 (bl-SnO_2) was deposited via spray pyrolysis deposition at 450 ºC from a solution of butyl-(tin chloride) in anhydrous ethanol at 1:10 volume ratio and then annealed at 500 °C for 30 min.

SnO_2 nanoparticle powders were used to synthesize the SnO_2 paste by following the method for making TiO_2 paste.[32] Briefly, 5 g SnO_2 nanoparticles were redispersed in 150 mL of anhydrous ethanol and mixed with 20 g terpineol and 15 g ethyl cellulose to prepare the SnO_2 paste. Mesoporous SnO_2 electrodes were obtained by spin-coating at 5,000 rpm for 30 s onto the bl-SnO_2 substrates using the SnO_2 paste diluted in ethanol (1:1, 1:3 and 1:5, weight ratio). After drying at 100 °C, the resulting mesoporous SnO_2 films were annealed at 500 °C for 30 min to remove the organic part. Some of SnO_2 films resulting from the SnO_2 paste diluted in ethanol (1:2, weight ratio) were treated in a 0.04 M aqueous solution of $TiCl_4$ at 60 °C for 1 h, rinsed with deionized water and annealed at 500 °C for 30 min. Prior to their use, the SnO_2 films were again dried at 500 °C for 30 min.

462 mg PbI_2 was dissolved in 1 ml DMF under stirring at 70 °C overnight, followed by filtering with 0.22 μm pore PVDF syringe filter. The solution was kept at 70 °C during the whole procedure. 25 μL PbI_2 solution was spin-coated on the mesoporous SnO_2 films at 3000 rpm for 20 s, and dried at 50 °C for 3 min and 100 °C for 5 min consecutively. After cooling to room temperature, 100 μL CH_3NH_3I solution in 2-propanol (10 mg ml^{-1}) was loaded on the PbI_2-coated SnO_2 films for 20 s, which was spun at 4000 rpm for 30 s and then dried at 100 °C for 5 min.

The spiro-MeOTAD HTM was deposited on the $SnO_2/CH_3NH_3PbI_3$ film by spin coating at 4,000 rpm for 30 s. The composition of spiro-MeOTAD HTM was 72.3 mg spiro-MeOTAD, 28.8μl TBP, and 17.5 μl of a solution of 520 mg/ml LiTFSI in acetonitrile in 1 ml chlorobenzene.

Finally, 60 nm-thick Au was thermally evaporated on top of the device to form the back contact. The active area of devices were 9 mm^2 determined by a black mask with dimension of 3 mm × 3 mm.

4.3. Characterization.

The surface morphology of the film was observed with a field emission scanning electron microscope (FE-SEM, sirion200, FEI Corp., Holland). The UV–vis spectrum of the films was obtained using a UV–vis spectrophotometer (U-3900H, HITACHI, Japan). The incident-photon-to-electron conversion efficiency (IPCE) measurement was conducted using a QE/IPCE measurement kit (Newport Corporation, CA). The current-voltage characteristics (*J-V* curves) were measured with a Keithley model 2420 digital source meter (Keithley Instruments, Inc.,USA) under the illumination of 100 mW/cm^2 (AM 1.5) provided by a solar simulator (solar AAA simulator, Oriel USA). Impedance spectra were measured with an electrochemical analyzer (Autolab 320, Metrohm, Switzerland) with a bias potential at 0.7 V. AC 20 mV perturbation was applied with a frequency from 1 MHz to 1 Hz. The obtained impedance spectra were fitted with ZView software (v2.8b, Scribner Associates, USA).

Acknowledgements

This work is financially supported by the National Basic Research Program of China under Grant No. 2011CBA00700 and the National Natural Science Foundation of China under Grant No. 21403247, 21173228, 61204075, 61404142.

Notes and references

[a] Key Laboratory of Novel Thin Film Solar Cells, Hefei Institutes of Physical Science, Chinese Academy of Sciences, Hefei, 230031, P. R. China.

[b] Department of Modern Physics, University of Science and Technology of China, Hefei 230026, P. R. China.

[c] Department of Chemical Engineering, University College London, London WC1E 7JE, UK.

[d] Beijing Key Laboratory of Novel Thin Film Solar Cells, State Key Laboratory of Alternate Electrical Power System with Renewable Energy Sources, North China Electric Power University, Beijing, 102206, P. R. China.

*Authors to whom correspondence should be addressed. Electronic mail: zhujzhu@gmail.com, junwangtang@ucl.ac.uk and sydai@ipp.ac.cn.

1. A. Kojima, K. Teshima, Y. Shirai and T. Miyasaka, *J. Am. Chem. Soc.*, 2009, 131, 6050-6051.
2. H.-S. Kim, C.-R. Lee, J.-H. Im, K.-B. Lee, T. Moehl, A. Marchioro, S.-J. Moon, R. Humphry-Baker, J.-H. Yum, J. E. Moser, M. Gratzel and N.-G. Park, *Sci. Rep.*, 2012, 2.
3. J. Burschka, N. Pellet, S.-J. Moon, R. Humphry-Baker, P. Gao, M. K. Nazeeruddin and M. Gratzel, *nature*, 2013, 499, 316-319.
4. S. D. Stranks, G. E. Eperon, G. Grancini, C. Menelaou, M. J. P. Alcocer, T. Leijtens, L. M. Herz, A. Petrozza and H. J. Snaith, *Science*, 2013, 342, 341-344.
5. H. Zhou, Q. Chen, G. Li, S. Luo, T.-b. Song, H.-S. Duan, Z. Hong, J. You, Y. Liu and Y. Yang, *Science*, 2014, 345, 542-546.
6. J. H. Im, C. R. Lee, J. W. Lee, S. W. Park and N. G. Park, *Nanoscale*, 2011, 3, 4088-4093.
7. J. M. Ball, M. M. Lee, A. Hey and H. J. Snaith, *Energy Environ. Sci.*, 2013, 6, 1739-1743.
8. H.-S. Kim, I. Mora-Sero, V. Gonzalez-Pedro, F. Fabregat-Santiago, E. J. Juarez-Perez, N.-G. Park and J. Bisquert, *Nat. Commun.*, 2013, 4, 2242.
9. G. Xing, N. Mathews, S. Sun, S. S. Lim, Y. M. Lam, M. Grätzel, S. Mhaisalkar and T. C. Sum, *Science*, 2013, 342, 344-347.
10. http://www.nrel.gov/ncpv/images/efficiency_chart.jpg, *The National Renewable Energy Laboratory (NREL)*, 2015.

11. W. Nie, H. Tsai, R. Asadpour, J.-C. Blancon, A. J. Neukirch, G. Gupta, J. J. Crochet, M. Chhowalla, S. Tretiak, M. A. Alam, H.-L. Wang and A. D. Mohite, *Science*, 2015, 347, 522-525.
12. H.-S. Kim, J.-W. Lee, N. Yantara, P. P. Boix, S. A. Kulkarni, S. Mhaisalkar, M. Grätzel and N.-G. Park, *Nano lett.*, 2013, 13, 2412-2417.
13. M. H. Kumar, N. Yantara, S. Dharani, M. Graetzel, S. Mhaisalkar, P. P. Boix and N. Mathews, *Chem. Comm.*, 2013, 49, 11089-11091.
14. J. You, Z. Hong, Y. Yang, Q. Chen, M. Cai, T.-B. Song, C.-C. Chen, S. Lu, Y. Liu and H. Zhou, *ACS Nano*, 2014, 8, 1674-1680.
15. K. Wojciechowski, M. Saliba, T. Leijtens, A. Abate and H. J. Snaith, *Energy Environ. Sci.*, 2014, 7, 1142-1147.
16. D. Bi, S.-J. Moon, L. Haggman, G. Boschloo, L. Yang, E. M. J. Johansson, M. K. Nazeeruddin, M. Gratzel and A. Hagfeldt, *RSC Adv.*, 2013, 3, 18762-18766.
17. X. Zhang, Z. Bao, X. Tao, H. Sun, W. Chen and X. Zhou, *RSC Adv.*, 2014, 4, 64001-64005.
18. K. Manseki, T. Ikeya, A. Tamura, T. Ban, T. Sugiura and T. Yoshida, *RSC Adv.*, 2014, 4, 9652-9655.
19. A. N. Green, E. Palomares, S. A. Haque, J. M. Kroon and J. R. Durrant, *J. Phys. Chem. B*, 2005, 109, 12525-12533.
20. A. Kay and M. Grätzel, *Chem. Mater.*, 2002, 14, 2930-2935.
21. M. Gratzel, *nature*, 2001, 414, 338-344.
22. S. Gubbala, V. Chakrapani, V. Kumar and M. K. Sunkara, *Adv. Funct. Mater.*, 2008, 18, 2411-2418.
23. M. K. I. Senevirathna, P. K. D. D. P. Pitigala, E. V. A. Premalal, K. Tennakone, G. R. A. Kumara and A. Konno, *Sol. Energ. Mat. Sol. C.*, 2007, 91, 544-547.
24. H. J. Snaith and C. Ducati, *Nano lett.*, 2010, 10, 1259-1265.
25. J.-H. Im, I.-H. Jang, N. Pellet, M. Grätzel and N.-G. Park, *Nat. Nano.*, 2014, 9, 927-932.
26. F. Huang, Y. Dkhissi, W. Huang, M. Xiao, I. Benesperi, S. Rubanov, Y. Zhu, X. Lin, L. Jiang, Y. Zhou, A. Gray-Weale, J. Etheridge, C. R. McNeill, R. A. Caruso, U. Bach, L. Spiccia and Y.-B. Cheng, *Nano Energy*, 2014, 10, 10-18.
27. G. E. Eperon, V. M. Burlakov, P. Docampo, A. Goriely and H. J. Snaith, *Adv. Funct. Mater.*, 2014, 24, 151-157.
28. J.-H. Im, H.-S. Kim and N.-G. Park, *APL Materials*, 2014, 2, -.
29. E. M. Barea, M. Shalom, S. Giménez, I. Hod, I. Mora-Seró, A. Zaban and J. Bisquert, *Journal of the American Chemical Society*, 2010, 132, 6834-6839.
30. V. González-Pedro, X. Xu, I. Mora-Seró and J. Bisquert, *ACS Nano*, 2010, 4, 5783-5790.
31. M. A. Hossain, J. R. Jennings, Z. Y. Koh and Q. Wang, *ACS Nano*, 2011, 5, 3172-3181.
32. L. H. Hu, S. Y. Dai, J. Weng, S. F. Xiao, Y. F. Sui, Y. Huang, S. H. Chen, F. T. Kong, X. Pan and L. Y. Liang, *J. Phys. Chem. B*, 2007, 111, 358-362.

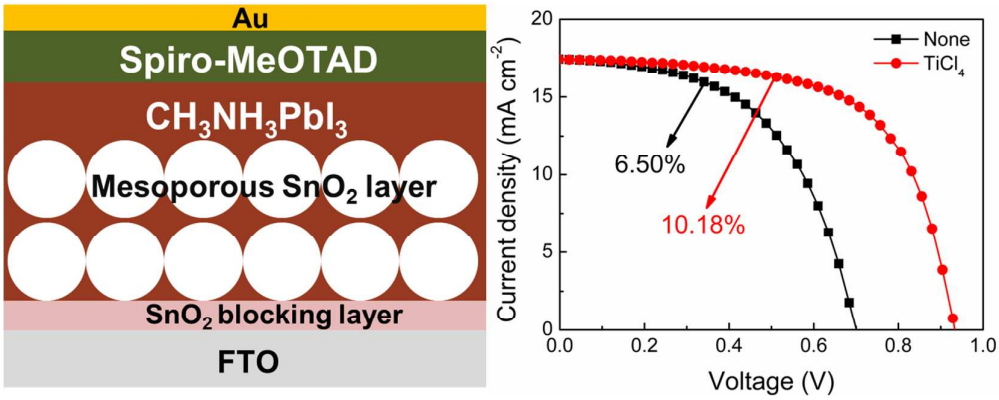

Mesoporous SnO_2 electrode is firstly introduced in the $CH_3NH_3PbI_3$ perovskite solar cell as electron-transporting materials and scaffold layers. The device exhibit an over 10% power conversion efficiency by optimizing the SnO_2 film thickness and treating the SnO_2 nanoparticle surface with $TiCl_4$ aqueous solution